

Polarization singularities in the clear sky

M V Berry¹, M R Dennis^{1,3} and R L Lee Jr²

¹ H H Wills Physics Laboratory, Tyndall Avenue, Bristol BS8 1TL, UK

² Physics Department, U.S. Naval Academy, 566 Brownson Road, Annapolis, MD 21402, USA

E-mail: mark.dennis@physics.org

New Journal of Physics **6** (2004) 162

Received 20 September 2004

Published 9 November 2004

Online at <http://www.njp.org/>

doi:10.1088/1367-2630/6/1/162

Abstract. Ideas from singularity theory provide a simple account of the pattern of polarization directions in daylight. The singularities (two near the Sun and two near the anti-Sun) are points in the sky where the polarization line pattern has index $+1/2$ and the intensity of polarization is zero. The singularities are caused by multiple scattering that splits into two each of the unstable index $+1$ singularities at the Sun and anti-Sun, which occur in the single-dipole scattering (Rayleigh) theory. The polarization lines are contours of an elliptic integral. For the intensity of polarization (unnormalized degree), it is necessary to incorporate the strong depolarizing effect of multiple scattering near the horizon. Singularity theory is compared with new digital images of sky polarization, and gives an excellent description of the pattern of polarization directions. For the intensity of polarization, the theory can reproduce not only the zeros but also subtle variations in the polarization maxima.

It is not one of the least wonders of terrestrial physics, that the blue atmosphere which overhangs us, exhibits in the light which it polarises phenomena somewhat analogous to those of crystals with two axes of double refraction

Brewster D 1863 *Trans. R. Soc. Ed.* **23** 205–10

³ Present address: School of Mathematics, University of Southampton, Highfield SO17 1BJ, UK.

Contents

1. Introduction	2
2. Singularity theory for polarization directions: fingerprints in the sky	2
3. The elliptic integral in the sky	5
4. Intensity of polarization	6
5. Comparison with multiple-scattering calculations	8
6. Comparison with observation	9
7. Discussion	12
Acknowledgments	13
References	13

1. Introduction

Rayleigh's explanation [1, 2] of the polarization of clear-sky daylight, in terms of dipole radiation singly scattered by air molecules, would predict that light is unpolarized in the direction of the Sun or anti-Sun (anti-solar point), whichever is above the horizon. But observations had already demonstrated the existence of three unpolarized directions: above the Sun (the Babinet point), below the Sun (the Brewster point [3]) and above the anti-Sun (the Arago point), and hinted at a fourth point below the anti-Sun (the second Brewster point [4]). These unpolarized points typically lie within 10–20° of the Sun or anti-Sun. The deviations from the Sun and anti-Sun were later interpreted as a multiple-scattering effect, which splits into two each of the unpolarized points from the single-scattering theory [5]; this approach has been considerably elaborated [6]–[8]. Extensive observations have been made of the patterns of direction and intensity of polarization [9]–[13].

Our purpose here, complementing previous studies based on scattering theory, is to understand the polarization of daylight as a manifestation of geometric singularity theory. This approach is based on the recognition that directions where the light is unpolarized are also 'fingerprint' singularities of the pattern of polarization directions. An individual fingerprint is illustrated in figure 1(a) and a pair in figure 1(b). Singularity theory not only enables an immediate qualitative understanding of the patterns but also suggests a simple quantitative theory (section 2), involving a minimum of formalism and applicable globally as well as locally. The global pattern of polarization lines can be generated as contours of an elliptic integral (section 3). A straightforward extension (section 4) gives the intensity of polarization. The theory agrees well with much more elaborate multiple-scattering calculations (section 5), as well as with new digital images (section 6) of the polarization of the sky.

2. Singularity theory for polarization directions: fingerprints in the sky

Imagine for a moment that the Earth is transparent, so that the whole sky sphere is illuminated. Then the existence and nature of four polarization singularities can be anticipated on the basis of topology. The polarization directions constitute a line field, whose singularities can be described by their index: the signed number of rotations of the field in a circuit of the singularity. By

● polarization singularities ● Sun or anti-Sun

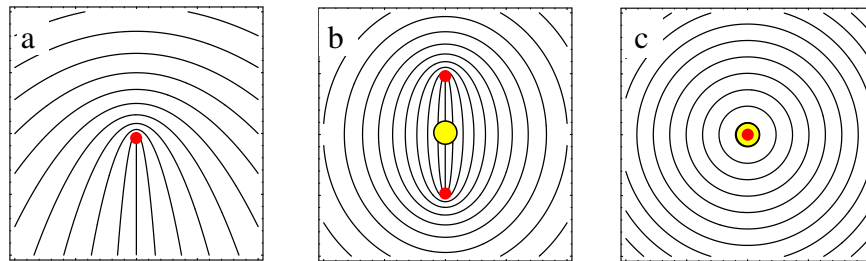


Figure 1. (a) Polarization lines near an individual singularity with index $+1/2$, described by (2.2) and calculated using (3.3). (b) Polarization lines near a pair of singularities, described by (2.4) and calculated using (3.4). (c) Circular polarization lines near the Sun or anti-Sun, according to the single-scattering (Rayleigh [1]) theory (2.3).

the ‘hairy ball theorem’ [14] of elementary topology, the total index of the singularities on a sphere (Euler characteristic) is $+2$ (two examples, generalizable by perturbation arguments, are the patterns of parallels of latitude or meridians of longitude, each of which has singularities of index $+1$ at the poles). Polarization lines (whose tangent gives the direction of polarization at any point), are unoriented (the electric fields \mathbf{E} and $-\mathbf{E}$ represent the same state of polarization) and for these the stable singularities have index $\pm 1/2$. The simplest possibility is for the singularities to be similar, in which case there are four of them, each with the ‘fingerprint’ pattern with index $+1/2$ (figure 1(a)). The singularities are arranged in two pairs (one is shown in figure 1(b)) approximately centred on the Sun and the anti-Sun.

Of course the Earth is not transparent, so at most two of the singularities are above the horizon at any time, and the singularity below the anti-Sun, apparently hinted at by Brewster [4], is not easy to see (it has recently been unambiguously observed from the air [11]).

To further understand the singularity structure, a perturbation argument is helpful. This starts from the simple single-scattering picture for polarization directions, in which light coming from a point P in the sky (representing a direction of arrival) is linearly polarized, with its electric field perpendicular to the arc connecting P to the Sun or anti-Sun (whichever is closest). The corresponding polarization lines are circles (figure 1(c)) centred on the Sun and anti-Sun, with maximum polarization occurring on the solar equator, which is the great circle comprising points at 90° to the Sun. Therefore, in this unperturbed picture the Sun and anti-Sun are singularities of the polarization lines, each with index $+1$.

But singularities of index $+1$ are unstable. Under perturbation—here double and higher-order multiple scattering—each index $+1$ singularity splits into two singularities with index $+1/2$ (figure 1(b)). Symmetry requires that the splitting is either along the solar meridian (the line connecting the Sun to the zenith) or perpendicular to it. In fact the former occurs, because the dominant contribution to multiple scattering, namely double scattering, is approximately vertically polarized and stronger alongside the Sun than directly above and below it. Thus, multiple-scattering polarization can be distinguished from single-scattering polarization only when the latter is both weak and horizontal, that is, along meridians near the Sun and anti-Sun (van de Hulst [5] attributes this argument to Soret).

To describe the patterns quantitatively, it is convenient to represent points P on the sky sphere by cartesian coordinates x, y or plane polar coordinates r, ϕ in the plane corresponding to the stereographic projection of P [15], and to represent x, y and r, ϕ by the complex combinations $\zeta = x + iy = r \exp(i\phi)$. We can choose the origin $\zeta = 0$ to represent either the Sun (or anti-Sun), or the zenith with the Sun on the y -axis (so the circle with elevation θ corresponds to $r = (1 - \tan(\theta/2))/(1 + \tan(\theta/2))$), in which case the visible hemisphere is the unit disk $r < 1$. The point antipodal to ζ is $-1/\zeta^*$. Polarization can be represented by the complex (unnormalized) Stokes parameter [16]. In terms of field components in the cartesian sky basis, this is

$$\begin{aligned} w(\zeta) &= \langle (E_x + iE_y)^2 \rangle = \langle E_x^2 \rangle - \langle E_y^2 \rangle + 2i\langle E_x E_y \rangle \\ &= |w(\zeta)| \exp\{2i\gamma(\zeta)\}, \end{aligned} \quad (2.1)$$

where the average is over all the scattered waves arriving from the point ζ . Then $|w(\zeta)|$ represents the intensity of polarization, and $\gamma(\zeta)$ gives the orientation of the polarization direction relative to the x -axis in the sky.

A related representation of polarization is obtained by dividing w by the daylight intensity $\langle E_x^2 \rangle + \langle E_y^2 \rangle$; the modulus of this normalized quantity is then the familiar degree of polarization, and its real and imaginary parts are the familiar normalized Stokes parameter. We avoid this normalization, because the complicated distribution of daylight intensity [17] is irrelevant to our concerns here. Another common practice is to define the polarization directions relative to zenith-centred polar, rather than cartesian, coordinates; we avoid this too, because it introduces a misleading apparent singularity at the zenith (cf section 5 and figure 4 below).

Each individual polarization singularity, with index $+1/2$, corresponds to a simple zero of $w(\zeta)$. This follows from the simplest local representation

$$w(\zeta) \propto \zeta = r \exp\{2i(\frac{1}{2}\phi)\}, \quad (2.2)$$

according to which the polarization direction γ makes a half-rotation ($\Delta\gamma = +\pi$) during a circuit $\Delta\phi = +2\pi$ of the singularity (figure 1(a)). (Poles of $w(\zeta)$ would correspond to singularities with index $-1/2$, which do not occur in the sky.)

On the unperturbed (single-scattering) theory, two singularities degenerate to give one with index $+1$, which is simply represented by a double zero:

$$w(\zeta) \propto -\zeta^2 = r^2 \exp\{2i(\phi - \pi/2)\}, \quad (2.3)$$

where the polarization lines are circles (figure 1(c)).

The degeneracy can be resolved by the simplest perturbation, namely the addition of a constant, that is

$$w(\zeta) \propto -(\zeta^2 + A^2), \quad (2.4)$$

with zeros at $\zeta = \pm iA$, that is $y = \pm A$, corresponding to polarization singularities above (–) and below (+) the Sun or above (+) and below (–) the anti-Sun, with angular separation $\delta = 4 \arctan A$ (figure 1(b)). Within this framework, the possibility that the distances of the two singularities from the Sun or anti-Sun might be slightly different can be accommodated by the further addition of a linear term.

The local behaviour (2.2), representing a single polarization singularity, and the semi-local behaviour (2.4), representing a split pair of singularities, can be globalized to include the whole sky by simply incorporating an antipodal pair of zeros:

$$w(\zeta) \propto -(\zeta^2 + A^2)(\zeta^2 + 1/A^2). \quad (2.5)$$

As we shall see, this represents the polarization pattern in Sun-centred coordinates. In zenith-centred coordinates, for Sun elevation α , that is at $\zeta = iy_S = i(1 - \tan(\alpha/2))/(1 + \tan(\alpha/2))$, the singularities are at

$$\zeta_+ = i \frac{(y_S + A)}{(1 - Ay_S)}, \quad \zeta_- = i \frac{(y_S - A)}{(1 + Ay_S)}, \quad -1/\zeta_+^*, \quad \text{and} \quad -1/\zeta_-^*. \quad (2.6)$$

Thus, the whole pattern of polarization lines can be represented by

$$w(\zeta) \propto (\zeta - \zeta_+)(\zeta - \zeta_-)(\zeta + 1/\zeta_+^*)(\zeta + 1/\zeta_-^*). \quad (2.7)$$

Here ζ_+ and ζ_- represent singularities below (Brewster) and above (Babinet) the Sun, respectively and $1/\zeta_+^*$ and $1/\zeta_-^*$ represent singularities above (Arago) and below the anti-Sun, respectively.

Equation (2.7) represents the minimal theory that correctly incorporates the singularities. The undetermined ingredients are the locations ζ_{\pm} of two of the singularities (or alternatively, in the perturbation picture, the Sun elevation α and the splitting $2A$), which must be supplied by observation or by a multiple-scattering calculation. Of course the minimal theory is approximate. One important feature of the approximation is the representation of $w(\zeta)$ as an analytic function, where the dependence on sky position x, y is through the combination $\zeta = x + iy$ alone, rather than some other combination of $\text{Re } \zeta$ and $\text{Im } \zeta$. For small splittings A , this is accurately close to the singularities, because the constant in (2.4) is the simplest perturbation and the form ζ^2 in (2.3) is an inevitable consequence of the circularity of the polarization lines in the unperturbed Rayleigh theory. However, we will see that (2.7) is also an accurate global approximation and for large A .

3. The elliptic integral in the sky

(Readers not interested in the calculation of the polarization lines can skip this section.)

It is convenient to represent the polarization lines as contours of a function $g(\zeta)$, rather than as a swarm of disconnected short line segments. (These polarization lines, analogous to streamlines in a flow, should be distinguished from the contours of constant γ , namely the ‘isogyres’—see section 5 and [18].) A pleasant consequence of representing polarization by the analytic function $w(\zeta)$ is that $g(\zeta)$ can be written in the simple form

$$g(\zeta) = \text{Im} \int^{\zeta} \frac{d\zeta_1}{\sqrt{w(\zeta_1)}} \quad (3.1)$$

(the lower limit is arbitrary). Its justification, originating in (2.1), is as follows:

$$\begin{aligned} \text{contours of } g &\Rightarrow dg(\zeta) = 0 = \text{Im} \frac{d\zeta}{\sqrt{w(\zeta)}} \propto \text{Im}[(dx + idy) \exp(-i\gamma)] \\ &= -dx \sin \gamma + dy \cos \gamma \propto \frac{dy}{dx} - \tan \gamma. \end{aligned} \quad (3.2)$$

For the isolated singularity (2.2), this gives the polarization lines

$$\operatorname{Im} \int^{\zeta} \frac{d\zeta_1}{\sqrt{-i\zeta_1}} = \operatorname{Re} \sqrt{y - ix} = \text{constant } K, \quad \text{i.e. } y = K^2 - \frac{x^2}{4K^2}, \quad (3.3)$$

i.e. a family of parabolas (figure 1(a)). For the pair (2.4), the lines are

$$\operatorname{Im} \int^{\zeta} \frac{d\zeta_1}{\sqrt{-(\zeta_1^2 + A^2)}} = \operatorname{Re} \left[\operatorname{arccosh} \left(\frac{ix - y}{A} \right) \right] = K \quad (3.4)$$

(figure 1(b)), representing a family of confocal ellipses with foci at the singularities. For the global representation (2.5), the lines, transformed to zenith-centred coordinates as in (2.6) and (2.7), are

$$\operatorname{Im} \int^{\zeta_t(\zeta, y_S)} \frac{d\zeta_1}{\sqrt{-(\zeta_1^2 + A^2)(\zeta_1^2 + 1/A^2)}} = A \operatorname{Im} F\{\arcsin(i\zeta_t(\zeta, y_S)/A), A^4\} = K, \quad (3.5)$$

where F denotes the elliptic integral of the first kind [19], and

$$\zeta_t(\zeta, y_S) = \frac{(\zeta + iy_S)}{(1 + i\zeta y_S)}. \quad (3.6)$$

Figure 2 illustrates these polarization lines.

4. Intensity of polarization

Consider now the more difficult question of modelling the intensity of polarization $|w(\zeta)|$ (i.e. the unnormalized degree, cf the remark below (2.1)). Locally, the zeros of the simple expressions (2.2)–(2.5) and (2.7) incorporate the fact that the singularities are points of zero polarization. Globally, however, (2.5) and (2.7) are inadequate, because although they include the desired antipodal symmetry in the polarization direction (phase of $w(\zeta)$), they fail to incorporate it into the modulus $|w(\zeta)|$. Alternatively stated, the formulae (2.5) and (2.7) are not the stereographic representations of smooth functions on a sphere. The modification of (2.7) is necessary to make the intensity of polarization antipodally invariant, that is

$$|w(-1/\zeta^*)| = |w(\zeta)|, \quad (4.1)$$

is

$$w(\zeta) = -\frac{4(\zeta - \zeta_+)(\zeta - \zeta_-)(\zeta + 1/\zeta_+^*)(\zeta + 1/\zeta_-^*)}{(1 + r^2)^2 |\zeta_+ + 1/\zeta_+^*| |\zeta_- + 1/\zeta_-^*|}. \quad (4.2)$$

The factors within the modulus signs in the denominator have been chosen so that the maximum value of $|w|$ is unity.

In fact, this formula for the intensity of polarization is exactly that proposed by Brewster in 1847 [3] to represent the degree of polarization. His expression was written in

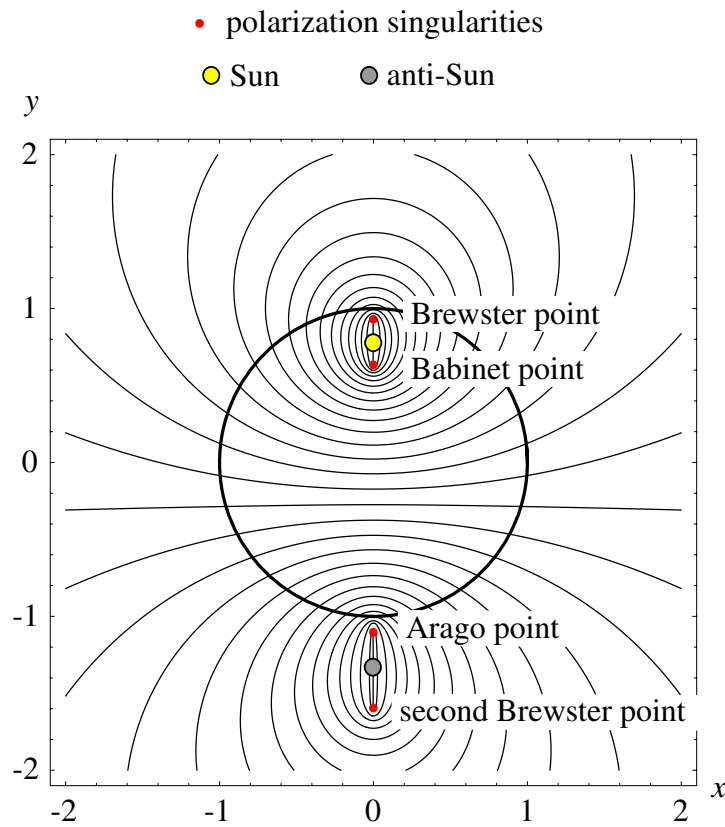


Figure 2. Polarization lines in the stereographic plane, for the Sun elevation $\alpha = 15^\circ$, with the singularities split by $\delta = 4 \arctan A = 12^\circ$, calculated from the model (2.7) using (3.5); the thick circle represents the horizon.

trigonometric form—natural for the intensity of polarization though not for the polarization direction—and is

$$|w(\zeta)| = |\sin \theta_{P+} \sin \theta_{P-}|, \quad (4.3)$$

where θ_{P+} and θ_{P-} are the angular distances between the sky point P (represented by ζ) and any two non-antipodal polarization singularities (e.g. the two above and below the Sun). In effect, our procedure of working with the complex sky coordinate ζ and the complex polarization $w(\zeta)$ incorporates the polarization directions into Brewster's model.

Our emphasis here is on the polarization singularities, namely the zeros of $|w(\zeta)|$, for which (4.2) and (4.3) work perfectly. A more discriminating test of models for $|w(\zeta)|$ is their ability to reproduce the points of maximum polarization, and here Brewster's model fails—as he was aware [3]—by predicting maxima on the horizon, at the two points 90° from the singularities (figure 3(a)). In fact, there seem to be no polarization maxima on the horizon, the probable reason being depolarization from the strong multiple scattering near the horizon. Instead, observations indicate either one maximum at the intersection of the solar meridian and solar equator or two maxima that are nearly equidistant from the solar meridian along the solar equator (as in figure 7 later). One remedy (also envisaged by Brewster) is to modify (4.2), for example by multiplication

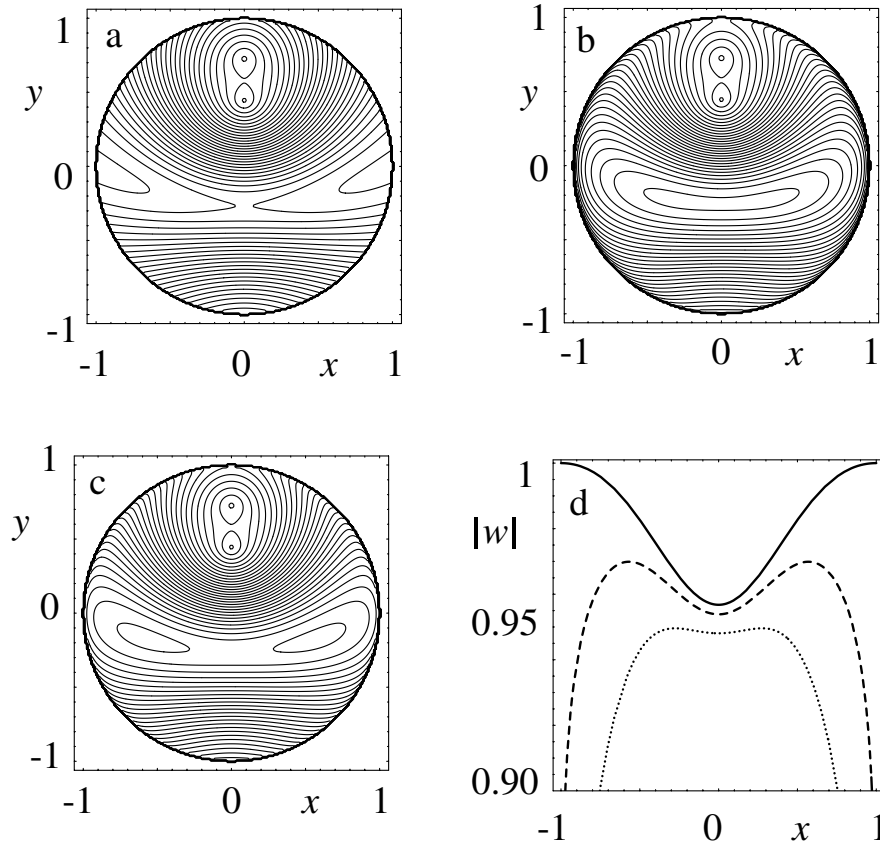


Figure 3. (a)–(c) Contours of intensity of polarization $|w(\zeta)|$ in the stereographic plane, for the Sun elevation 30° and splitting $\delta = 24^\circ$; (a) calculated from (4.2) with no horizon correction, i.e. $h(r) = 1$; (b) from (4.3) with horizon correction $h_1(r) = \cos(\pi r/2)^{1/10}$ and (c) $h_2(r) = \cos(\pi r/2)^{1/30}$. (d) $|w|$ on the solar equator; —, $h = 1$; ·····, $h = h_1$; - - - - - , $h = h_2$.

by an ad hoc horizon function $h(r)$ with the properties

$$h(0) = 1 \text{ (zenith);} \quad h(1) = 0 \text{ (horizon).} \quad (4.4)$$

The polarization maxima are very sensitive to $h(r)$, because the maxima on the horizon, predicted by Brewster's theory (4.3), are weak for small separations δ : the ratio of the minimum value of $|w|$ on the solar equator (where the meridian intersects it) and on the horizon (where $|w| = 1$), is $\cos^2(\delta/2)$ (≈ 0.93 for $\delta = 30^\circ$). Slight differences in the form of $h(r)$ can generate either one maximum (figure 3(b)) or two (figure 3(c)).

5. Comparison with multiple-scattering calculations

Extensive multiple-scattering calculations of polarization directions were made by Chandrasekar and Elbert [8], starting from general radiative transfer theory [6]. For several elevations of the Sun, they plot the contours (isogyres) corresponding to polarization directions making 45° with the meridian at the given azimuth ('local vertical'); these are the 'neutral lines', separating regions

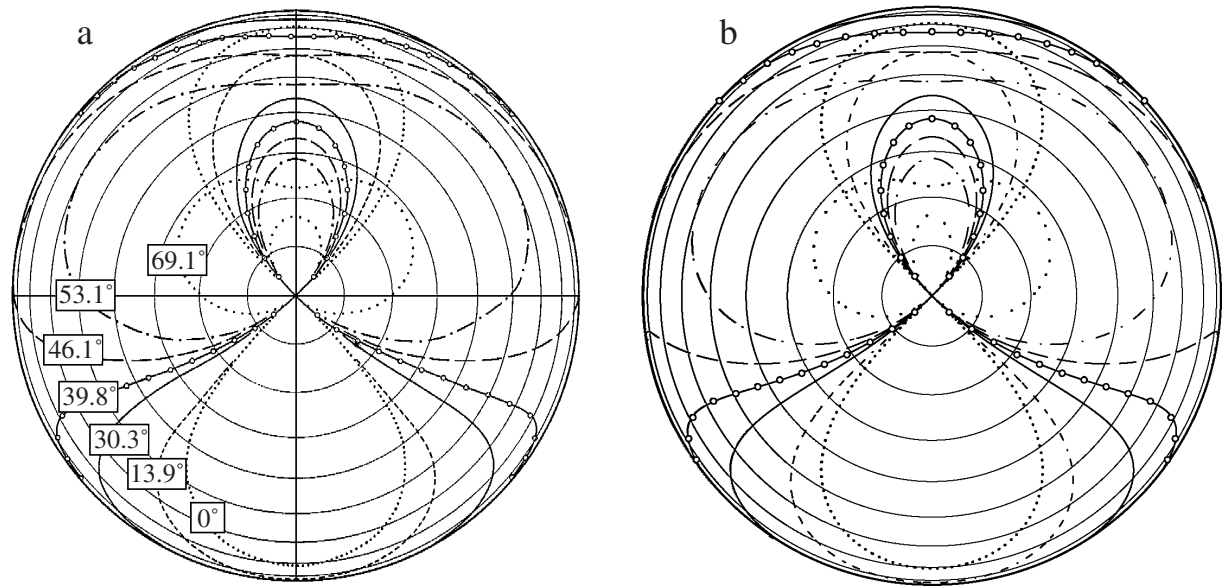


Figure 4. (a) Neutral lines (contours of polarization directions at $\pm 45^\circ$ to the vertical), calculated by multiple-scattering theory [8], for the indicated Sun elevations; (b) neutral lines for the same Sun elevations as in (a), calculated on the simple theory based on (2.7) and (5.1) with the same locations of the singularities as in (a). The circles are almaccantars (loci of constant elevation), spaced at 10° intervals; radial distance is proportional to $\cos(\text{elevation angle})$.

conventionally referred to as having positive and negative polarization. Figure 4(a) shows the neutral lines, which as Chandrasekar and Elbert demonstrated are in good agreement with data from observations by Dorno.

Now we compare the multiple-scattering theory with the simple theory of section 2, based on the quartic polynomial (2.7), whose structure is determined entirely by the locations of the polarization singularities. By transforming (2.1) to polar coordinates, it is easy to see that the neutral lines are the contours

$$\gamma(\zeta) - \phi = \frac{1}{2} \arg w(\zeta) - \phi = \pm \frac{1}{4}\pi. \quad (5.1)$$

These contours are shown in figure 4(b). Evidently the agreement with the much more elaborate multiple-scattering theory is excellent.

Hannay [20] has recently shown that the complexities of the full (all-orders) multiple-scattering theory can be greatly reduced by caricaturing the atmosphere as a thin flat sheet, exploiting the fact that it is much less deep than wide. This approach gives a physical justification for our topologically-motivated quartic polynomial (2.7).

6. Comparison with observation

Although there have been many measurements of the polarization of skylight, we know only one observation [10] that clearly shows the form of polarization lines near one of the singularities that we are emphasizing.

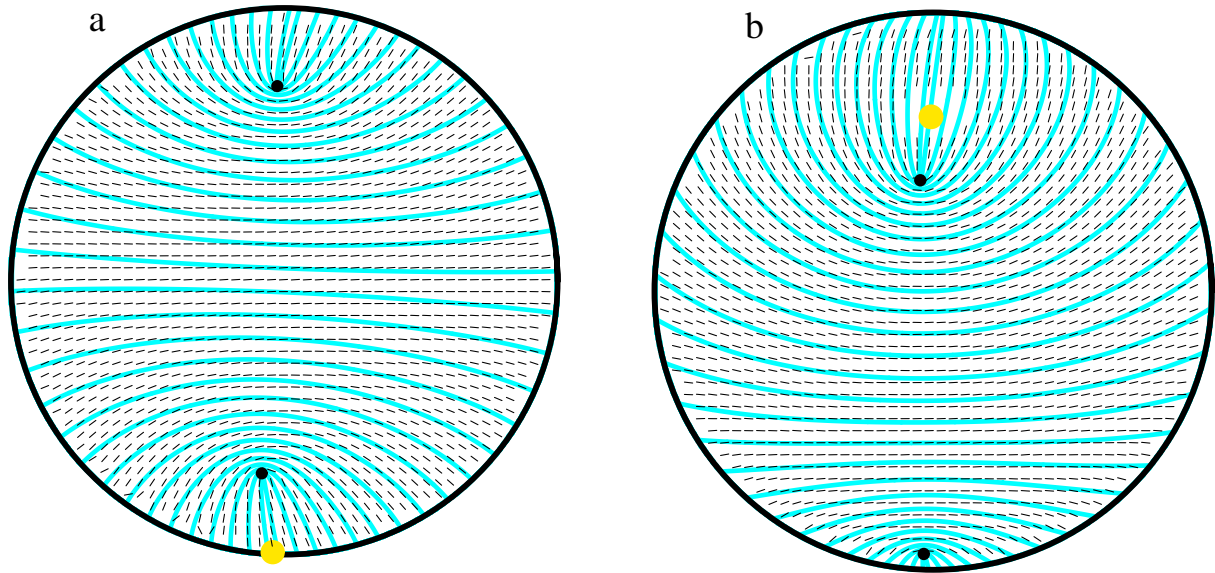


Figure 5. Observed (black line segments) and predicted (blue lines) polarization directions (the radial coordinate is proportional to zenith angle). Both observations were made at the United States Naval Academy in Annapolis, MD, at unrefracted Sun elevations of (a) -0.71° and (b) 33.7° , on 3 November 2003. The Sun's location is marked by a yellow disc, and observations are missing near it in (b).

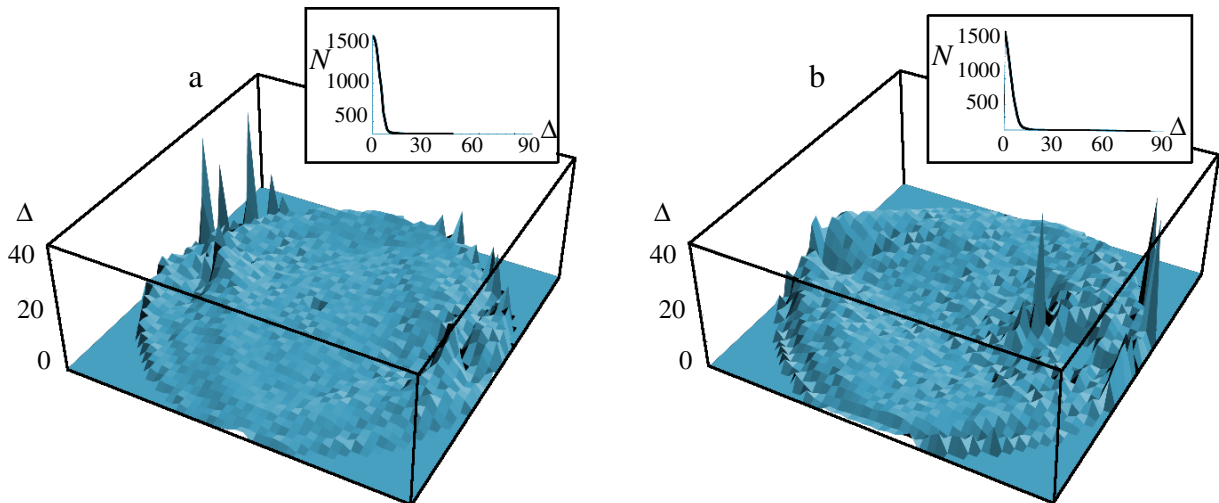


Figure 6. Angular deviations between the observed and predicted polarization directions, corresponding to figures 5(a) and (b). The three-dimensional plots show the spatial distribution of the deviations, and the graphs (inset) show the number N of data points with $|\text{deviations}| > \Delta$ (in degrees).

In order to make detailed comparisons of our theory with real clear skies, in figures 5–7 we show maps of the direction and intensity of skylight polarization. We calculate the observed contours of $\gamma(\zeta)$ and $|w(\zeta)|$ in figures 5–7 by extending techniques developed earlier for normal field-of-view lenses [13] to fisheye lenses. A Nikon E5000 digital camera with an FC-E8 fisheye

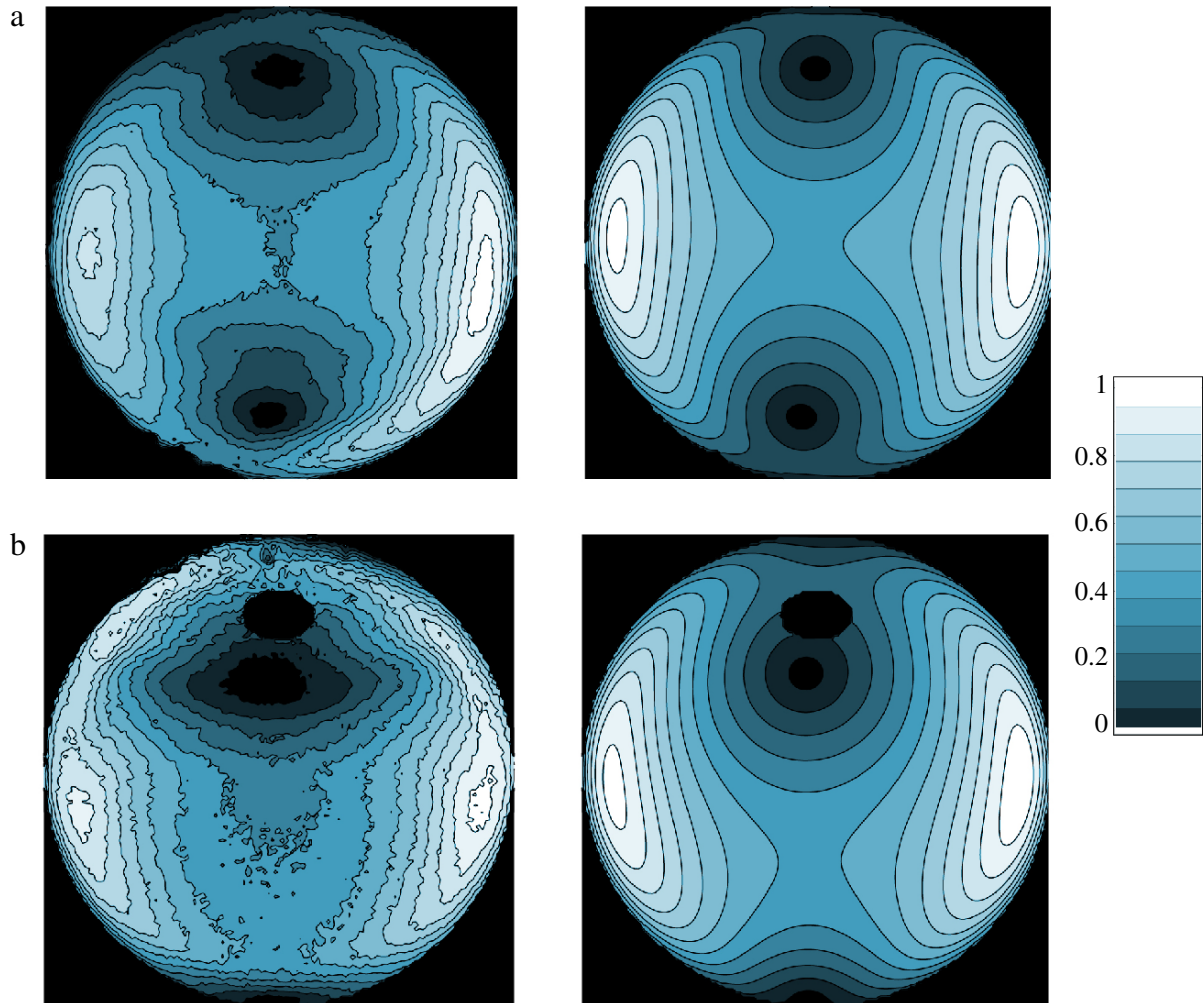


Figure 7. Contour plots of intensity of polarization corresponding to figures 5(a) and (b). For each case, the left-hand picture is the observation and the right-hand picture is the theory, namely $|w(\zeta)|$ (equations (4.2) and (4.3)) multiplied by the horizon function (6.1) (in (b), the black regions above the singularity correspond to the unmeasured neighbourhood of the Sun).

converter was used to take four different polarized photographs of each of the two clear-sky cases at the United States Naval Academy in Annapolis, Maryland. We extract relative radiance data from these photographs by adapting existing algorithms for radiometric calibration of digital images [21]. To prevent flare within the fisheye lens during the day, a small shield was used to occult the Sun and the immediate circumsolar region [11, 12]. In figure 5(b), this occulted area appears as a gap in the dashed lines of observed $\gamma(\zeta)$. Although the clear sky in each fisheye photograph occupies an area ~ 690 pixels on a side, in figure 5 we sample $\gamma(\zeta)$ only at every 15th row and column.

For greater radiometric accuracy and sensitivity, we integrate all radiances across the visible spectrum. This brings the disadvantage that dispersion will slightly obscure the details near the singularities, whose location is wavelength-dependent [10]. However, we know from geometry the arrangement of polarization lines close to the singularities, so the main purpose of the

comparison with experiment is to assess the accuracy of the global expression (2.7) away from the singularities, where dispersion is a small effect.

Consider first the maps of polarization directions that are plotted in figure 5. These maps show both the measured directions and the directions predicted by the simple theory of section 2, with the locations of the singularities in (2.7) fitted from the observation. Visual inspection indicates that the theoretical and observed patterns agree rather well, with the greatest deviations occurring near the singularities.

For quantitative comparisons, we show in figure 6 the deviations between the predicted and observed polarization directions, as spatial and cumulative plots. The spatial plots confirm that the deviations are small except near the singularities, and the cumulative plots show that the typical deviations (median values) are about 5° , and 90% of the deviations are less than 8° .

Figure 7 is a comparison of the measured intensity of polarization (left-hand pictures) with the theory (right-hand pictures). The theory incorporates the horizon function $h(r)$ discussed in section 4. We chose $h(r)$ by fitting a polynomial to the measured polarization intensity along the solar equator in figure 7(a). This horizon function, satisfying (4.4), is

$$h(r) = (1 + 0.35r^2 + 0.65r^4)(1 - r^2). \quad (6.1)$$

As can be seen, this is a good fit not only to figure 7(a) away from the solar equator, but also to the very different situation of figure 7(b).

7. Discussion

Singularities with index $+1/2$ occur elsewhere in polarization optics [22]–[24], and in other line fields, for example the ridges in fingerprints [25] and the director in liquid crystals [26]. Most notably, the global pattern of four singularities in figure 2, determined by the argument of the complex quartic polynomial (2.7), is identical to the pattern of directions of polarization of light in a transparent biaxial crystal without optical activity [23, 24] as a function of illumination direction; for crystals, the singularities are the optic axes. The quotation at the beginning of this paper indicates that this connection was appreciated by Brewster. Brewster's intuition is doubly remarkable: his emphasis was on the intensity of sky polarization rather than on the direction, and he never accepted the wave picture of light that underlies both the crystal and the sky phenomena.

Although the skylight and crystal polarization patterns look identical, it is important to recognize that they differ in several ways. In the case of a crystal, there are two orthogonal polarizations for light propagating in each direction, whereas in the sky there is just one polarization. And in the crystal case, the light is perfectly linearly polarized, in contrast to the states of partial linear polarization in the sky.

The detailed distribution of polarization in the sky is complicated by several effects that we have not considered here, for example the scattering by tropospheric haze droplets and other large particles, light reflected by the ground or the sea, and the dependence of polarization patterns (including the locations of the singularities) on wavelength, and subtle effects near the horizon. Multiple-scattering theory can be elaborated to account for some of these effects. In our complementary approach, we have deliberately ignored these refinements, our purpose being to present the simplest framework in which the singularities appear with the correct structure.

Nevertheless, the simplest 'globalization', embodied in the quartic polynomial (2.7), agrees rather well with multiple-scattering theory and with observations. This might seem surprising,

but it is not unprecedented. In fluid mechanics, a similar globalization of the pattern of vortices and saddles in the flow between six rollers is also remarkably accurate [27]. These examples illustrate a more general point: global patterns are rather strongly constrained by the arrangement of local singularities.

Acknowledgments

We thank J H Hannay for several discussions. MVB is supported by the Royal Society, MRD by the Leverhulme Trust, RLL by United States National Science Foundation grant ATM-0207516 and by the United States Naval Academy's Departments of Physics and Mathematics.

References

- [1] Lord Rayleigh 1871 On the light from the sky, its polarization and colour *Phil. Mag.* **61** 107–20 and 274–9
- [2] van de Hulst H C 1981 *Light Scattering by Small Particles* (New York: Dover)
- [3] Brewster D 1847 On the polarization of the atmosphere *Phil. Mag.* **31** 444–54
- [4] Brewster D 1863 Observations of the polarisation of the atmosphere, made at St. Andrews in 1841, 1842, 1843, 1844, and 1845 *Trans. R. Soc. Edinb.* **23** 211–39
- [5] van de Hulst H C 1949 Scattering in atmospheres *The Atmospheres of the Earth and Planets* ed G P Kuiper (Chicago, IL: Chicago University Press) pp 49–111
- [6] Chandrasekar S 1950 *Radiative Transfer* (Oxford: Clarendon)
- [7] Chandrasekar S and Elbert D 1951 Polarization of the sunlit sky *Nature* **167** 51–4
- [8] Chandrasekar S and Elbert D 1954 The illumination and polarization of the sunlit sky on Rayleigh scattering *Trans. Am. Phil. Soc.* **44** 643–728
- [9] Sekera Z 1957 Light scattering in the atmosphere and the polarization of sky light *J. Opt. Soc. Am.* **47** 484–90
- [10] Horvath G, Gal J and Pomozi I 1998 Polarization portrait of the Arago point: video-polarimetric imaging of the neutral points of skylight polarization *Naturwiss.* **85** 333–39
- [11] Horvath G, Bernath B, Suhai B and Barta A 2002 Observation of the fourth neutral polarization point in the atmosphere *J. Opt. Soc. Am. A* **19** 2085–99
- [12] Gal J, Horvath G, Meyer-Rochow V B and Wehner R 2001 Polarization patterns of the summer sky and its neutral points measured by full-sky imaging polarimetry in Finnish Lapland north of the Arctic Circle *Proc. R. Soc. A* **457** 1385–99
- [13] Lee R L Jr 1998 Digital imaging of clear-sky polarization *Appl. Opt.* **37** 1465–76
- [14] Firby P A and Gardiner C F 1991 *Surface Topology* 2nd edn (Chichester: Ellis Horwood)
- [15] Needham T 1997 *Visual Complex Analysis* (Oxford: Oxford University Press)
- [16] Azzam R M A and Bashara N M 1977 *Ellipsometry and Polarized Light* (Amsterdam: North-Holland)
- [17] Coulson K L 1988 *Polarization and Intensity of Light in the Atmosphere* (Hampton: Deepak)
- [18] Born M and Wolf E 1959 *Principles of Optics* (London: Pergamon)
- [19] Wolfram S 1996 *The Mathematica Book* (Cambridge: Cambridge University Press)
- [20] Hannay J H 2004 Partial polarization of light from a thin sheet atmosphere in the sky (submitted to *New J. Phys.*)
- [21] Lee R L Jr 1988 Colorimetric calibration of a video digitizing system: algorithm and application *Color Res. Appl.* **13** 180–6
- [22] Nye J F 1999 *Natural Focusing and Fine Structure of Light: Caustics and Wave Dislocations* (Bristol: Institute of Physics Publishing)
- [23] Berry M V, Bhandari R and Klein S 1999 Black plastic sandwiches demonstrating biaxial optical anisotropy *Eur. J. Phys.* **20** 1–14
- [24] Berry M V and Dennis M R 2003 The optical singularities of birefringent dichroic chiral crystals *Proc. R. Soc. A* **459** 1261–92

- [25] Penrose R 1979 The topology of ridge systems *Ann. Hum. Gen.* **42** 435–44
- [26] Frank F C 1958 On the theory of liquid crystals *Faraday Sci. Discuss.* **25** 19–28
- [27] Berry M V and Mackley M R 1977 The six roll mill: unfolding an unstable persistently extensional flow *Phil. Trans. R. Soc. A* **287** 1–16